INCOM

Bright Ideas in Fiber Optics

# Measurement & Test Report

# LAPPD #25

## March 6, 2018

INCOM, INC.
294 Southbridge Road
Charlton, MA 01507-5238

Tel: (508) 909-2200
Fax: (508) 909-2323

## Packing

The LAPPD is wrapped in foil and placed in a Pelican case with antistatic foam (Figure 1). The foil helps manage static charging, which could be harmful to charge-sensitive electronics that will be attached to it. It also keeps unnecessary stray light from exciting the photocathode, and charging the entry MCP.

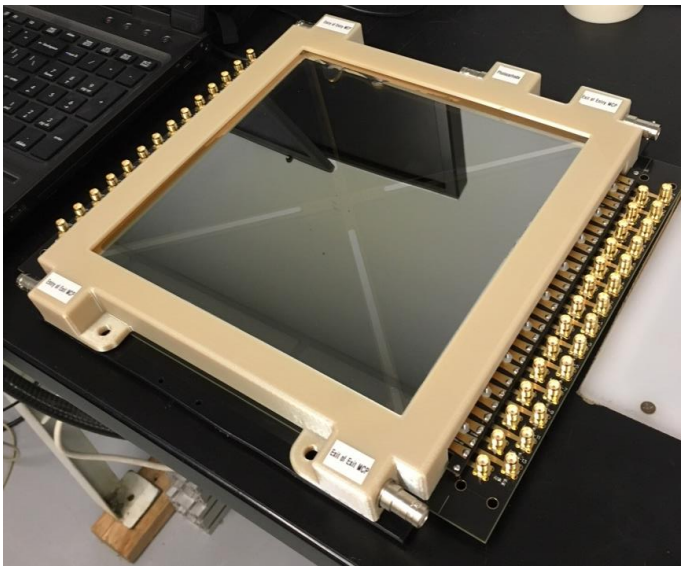

Figure 1. Left: The LAPPD is wrapped in foil to manage static charging, and to keep stray light from the photocathode. Right: the LAPPD is enclosed in an ultem housing with high voltage connectors, and mounted on a backplane for signal access.

## Connectivity

An ultem housing and a backplane are provided with each LAPPD (Figure 1). The backplane connects the strips to SMA connectors with near-50 ohm impedance. The ultem housing provides the high voltage connections. They consist of SHV panel mount connectors on the outside, and Mill-Max spring-loaded ball tip pins on the inside. The pins touch the high voltage pads on the LAPPD envelope. The 5 high voltage connectors are labeled according to their function. The shields on the SHV connectors simply terminate the high voltage cable shield, and minimize unwanted signal pickup in the detector. They do not close any high voltage current paths.

### High voltage connection diagram

The high voltages may be connected as shown in Figure 2 and 3 for maximum control of the LAPPD. This recommended approach separates the current paths of the entry and exit MCPs, so anomalies in either may

be detected. Additionally, the photocathode voltage may be controlled independently of the MCPs. Without changing the gain, the photocathode voltage may be increased, which will increase the gain somewhat as the photoelectrons acquire more energy before impacting the microchannel. Alternatively, it may be decreased so it is more positive than the entry side of the entry MCP. In this case, the photoelectrons will remain at the photocathode, and the MCP dark pulses may be observed. This state may also be used if an accidental exposure of the LAPPD to light is anticipated.

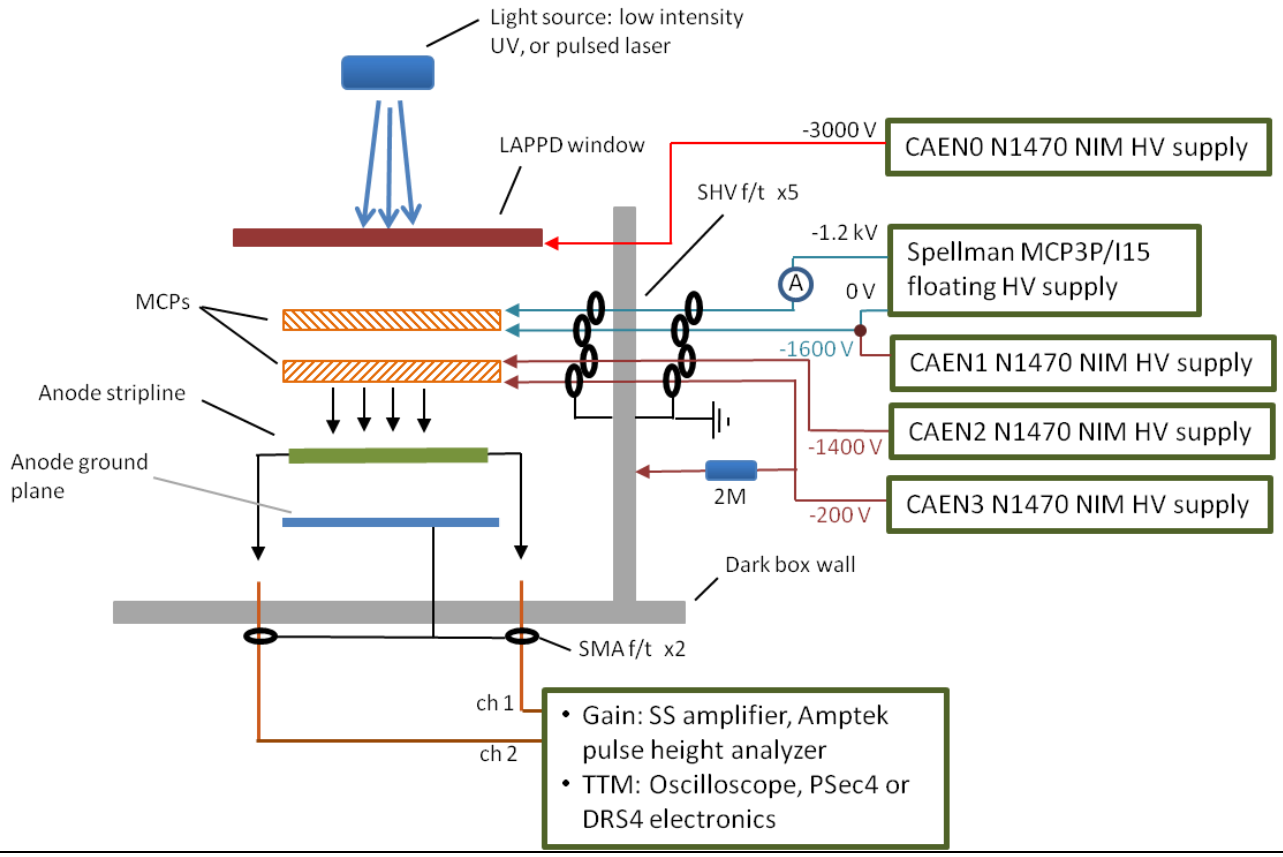


- Monitor MCP currents separately.
- Accommodate either orientation: high resistance MCP on the entry or exit side
- Don't close the strip current of the entry MCP through the exit MCP.

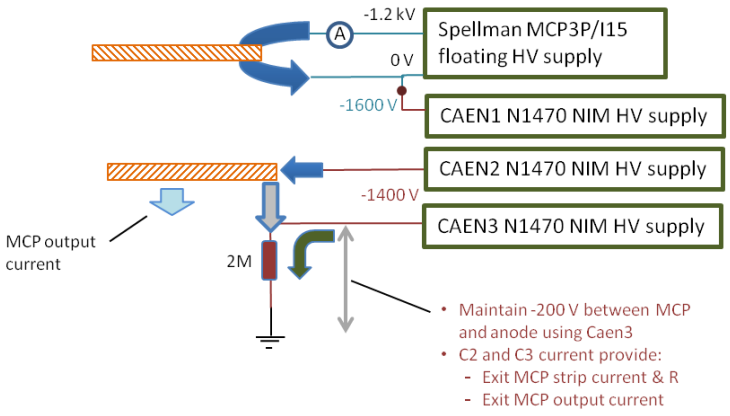


**Figure 2 Top:** The wiring diagram for high voltage and signals is shown for the LAPPD gain and timing testing at Incom. **Bottom:** A schematic shows the separation of the two MCP current paths, and the techniques used to separately measure the output current to the anode and the strip current through the exit MCP.

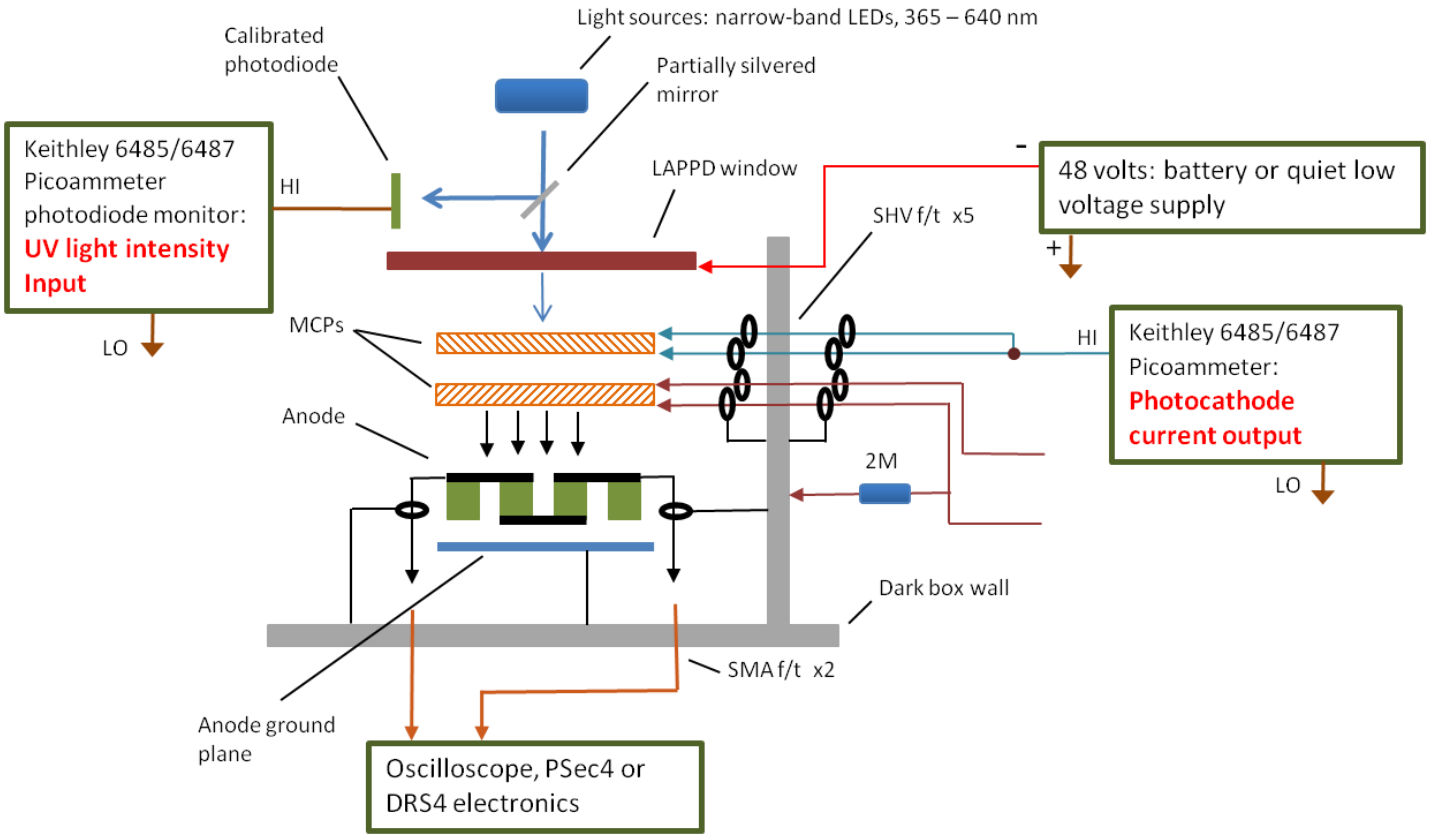


**Figure 3:** The wiring diagram for the QE measurement is shown. The exit MCP and the anode are not involved in this measurement. Instead, the entry MCP serves as the anode for the photocurrent.

**LAPPD #25 General Features and Parameters:**

| Feature | Parameter |
|---|---|
| Photodetector Material | Borosilicate Glass |
| Window Material | Fused Silica Glass |
| Photocathode Material | Multi-Alkali ($K_2NaSb$) |
| Spectral Response (nm) | 160-850 |
| Wavelength – Maximum Sensitivity (nm) | ≤ 365 nm |
| Photodetector Active Area Dimensions | 195mm X 195mm |
| • Minimum Effective Area | 34,989 mm^2 |
| • Active fraction with Edge Frame X-Spacers | 92% |
| Anode Data Strip Configuration | 28 silver strips, Width = 5.2 mm, gap 1.7 mm, nominal 50 Ω Impedance |
| Voltage Distribution | 5 taps for independent control of voltage to the photocathode and entry and exit of MCP |

### LAPPD # 25 Operational Ratings

| Parameter | Rating |
|---|---|
| Supply voltage Photocathode — Anodes (Volts) | Typical:<br>• 100V between MCP and photocathode<br>• 875 V/MCP<br>• 200 V between MCPs<br>• 200 V between MCP and anode<br>• Photocathode voltage is -2250 V<br>Recommended MCP V: 850/950 V/MCP (entry/exit)<br>Maximum: Photocathode voltage at -2900 V |
| Operating ambient temperature °C | TBD (nominal room temperature) |
| Storage temperature °C | TBD (nominal room temperature, avoid indium seal melt) |

### LAPPD Package / Housing Characteristics

| Parameter | Rating |
|---|---|
| Photodetector Physical Dimensions (L X W X Thkns, mm) | 230 x 220 x 22 |
| Photodetector Mounting Case | ULTEM or equivalent dielectric polymer |
| Photodetector Mounting Case Dimensions | 243 mm X 274 mm X 25.2 mm |
| Connectivity | Passive PC Interface Board ,<br>(300 mm X 264 mm X 1.6mm) |
| Overall Footprint, with Mounting Case & PC Interface Board | 300 mm X 274 mm X 26.8 mm |
| Shipping Container | Pelican Case + Cardboard Box + G-force indicators |

### LAPPD #25 Microchannel Plate (MCP) Features & Performance

| | |
|---|---|
| MCPs | Two Arranged in a Chevron Pair |
| Dimensions | 203 mm x 203 mm X 1.2 mm |
| MCP Substrate | Incom C5 Glass |
| Capillary Pore Diameter (µm)<br>Center to Center Pitch (µm) | 20<br>25 |
| Channel Length / diameter<br>Substrate Thickness (mm) | 60:1<br>1.2 |
| Bias Angle | 13 |
| Capillary Open Area Ratio | ≥64% |
| Resistive and Emissive Coatings | Chem 1, Applied via Atomic Layer Deposition (ALD) |

| | |
|---|---|
| Secondary Emission (SEE) Layer Material | MgO |
| Electrode Penetration – Input & Output (Pore Diameter) | 1 |
| MCP ID (Entry / Exit) | C00101-029 / C00101-006 |
| MCP Chevron Pair Gain (@ Measurement & Test) | 5E5 @900 Volts/MCP with variation σ = 7% around the mean |
| MCP resistance (Entry/Exit) | 10.7 / 14.2 MOhms at 875 V |
| Dark Counts | 0.45 Cts/S cm^2 at a threshold of 2.5E5 gain (40.5 fC)[A] |
| Max Voltage | 850/950 V/MCP recommended (entry/exit), -2900 volts at the photocathode maximum. |

LAPPD #25 Operating Performance

| Parameter | Performance |
|---|---|
| Photocathode Quantum efficiency | • Mean QE at 365 nm: 7.1%, with a std dev of 0.8%<br>• Mean QE @455 nm: 10.2% ± 1.5 |
| Photocathode QE Spatial Variability (σ) | 11% of the mean |
| Tile Dark Count rate per 13.5 cm^2 strip | 303 Hz, at 875 V per MCP, with 30 V on the photocathode, at a threshold of 7.3E5 gain (116 fC)[B] |
| LAPPD Gain | 7.5 $X10^6$ @ 850/950 V (entry/exit), with variation = σ ≤ 50% mean |
| | 6 $X10^6$ @ 900 V per MCP |
| Dark / Background Rate @ gains ≥ 0.5 PE, on a single 13.5 cm^2 strip | 0.0022 Hz/cm^2 with 50 volts on the photocathode and 850 V/MCP, with a threshold of 2.2E5 gain |
| On-strip (end-to-end time difference) Resolution | 37.5 pS |

### Functional Tests – Overview

Functional tests were performed on LAPPD 25 in a dark box that was fitted with a UV light source and signal acquisition hardware. Some of these tests were performed during the second Incom LAPPD Workshop held in January 2018. A summary of the results is shown below. The measurements include:

1. **MCP gain and intensity map prior to assembly**
2. **MCP resistance vs. voltage**
3. **LAPPD Photocathode QE spectrum and map**
4. **LAPPD Gain**
    - Gain vs. MCP voltage
    - Gain vs. photocathode voltage
    - Gain from waveform samplers
    - Gain vs. repetition rate
5. **LAPPD Dark rates vs. MCP and photocathode voltage**
6. **LAPPD Timing and Position**
    - Position along a strip, inferred from relative pulse arrival times at each end
    - Position across strips from centroiding

### MCP gain and intensity map prior to assembly

The gain of the MCPs prior to assembly is shown in Figure 4. The maps feature an X pattern of lower gain. This pair of MCPs was previously used in an earlier LAPPD, and went through thermal bake-out and scrubbing prior to being allocated for use in LAPPD 25. The overall pattern may be somewhat different now, since the MCPs experienced further scrub and thermal bake-out during the normal course of LAPPD #25 assembly process. No spatial gain map has been made of the completed device; however, a map similar to the QE map is planned for future devices.

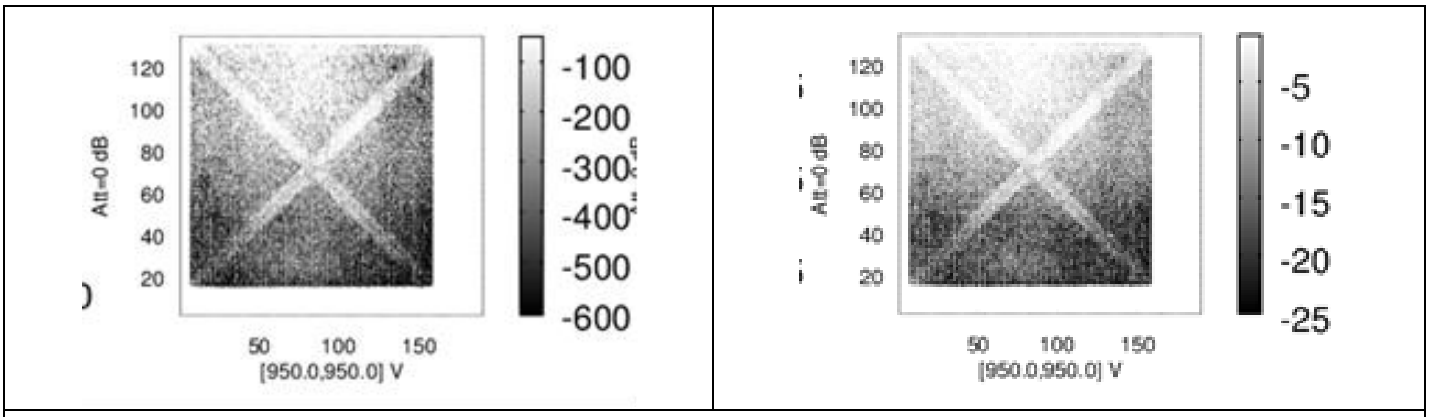


**Figure 4** - Left: Gain map for the LAPPD 25 MCPs prior to assembly at 950 V/MCP. Dark shading is higher gain. **Right:** Intensity map for the LAPPD 25 MCPs prior to assembly. Dark shading is higher intensity.

### MCP resistance vs. voltage

The MCP resistance is shown in Figure 5, as a function of voltage. They are non-ohmic, and their resistance decreases somewhat with increasing voltage. Some of this behavior may be attributed to warming, as the MCP resistance decreases with increasing temperature. The resistive film in this pair of MCPs is quite uniform, as the MCPs do not thermally run away. The low resistance is also advantageous for high rate operation. The variation of resistance with voltage in Figure 5 must be considered if a resistor divider network will be used to distribute high voltages.

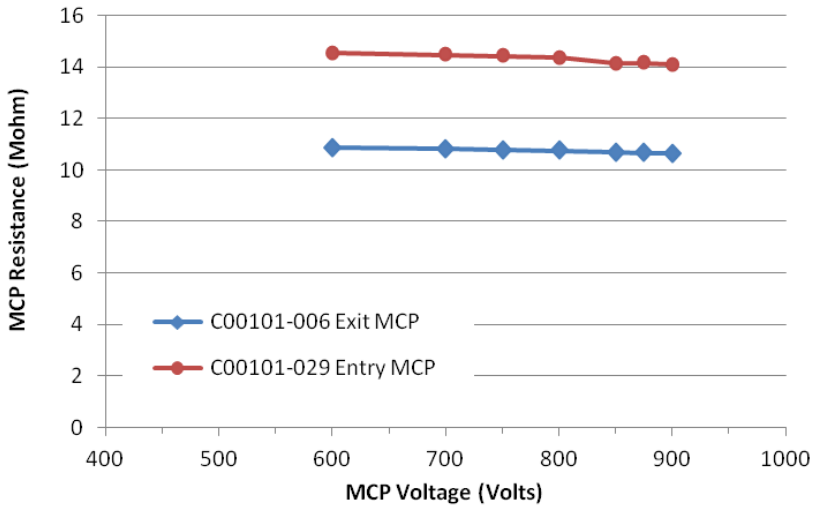


**Figure 5** - MCP resistances for LAPPD 25. C00101-029 is the entry MCP and C00101-006 is the exit MCP.

### LAPPD Photocathode QE spectrum and map

The quantum efficiency of the photocathode was measured across the LAPPD window by scanning a 365 nm UV LED in an XY pattern of 5 mm steps. The illumination on the window had a circular pattern with a 10 mm diameter. The intensity of the input light was measured with a Thorlabs SM1PD2A photodiode, and a Keithley 6485 picoammeter (see Figure 3). The photocurrent was collected by connecting both sides of the entry MCP to a Keithley 2400 picoammeter, with a 42 volt bias voltage between the MCP and the photocathode. The quantum efficiency is calculated from the ratio of these two quantities, less the dark current in each.

The UV LED source was stepped across the LAPPD window in 5 mm steps. At each step, the input light intensity was measured, as well as the resulting photocurrent. The QE map, measured at 365 nm, is shown in Figure 6. The average QE at 365nm was 7.1%, with a standard deviation of 0.8%. This calculation of the mean excluded the X-spacers and the low QE region in the upper right of the map in Figure 6. The X-spacers are visible in the map, although not quite dark because they are 6mm wide, but the UV spot size is 10 mm in diameter. A somewhat circular feature of unknown origin is apparent in the photocathode map at the right side, where the QE is lower than elsewhere.

The QE spectrum is also shown in Figure 6 (right), from a selected location, measured at 455 nm, measured for the sealed tile, immediately following fabrication. The peak may be there, or at a wavelength shorter than 365 nm. The mean QE for tile #25 at 455 nm was 10.2% ± 1.5%.

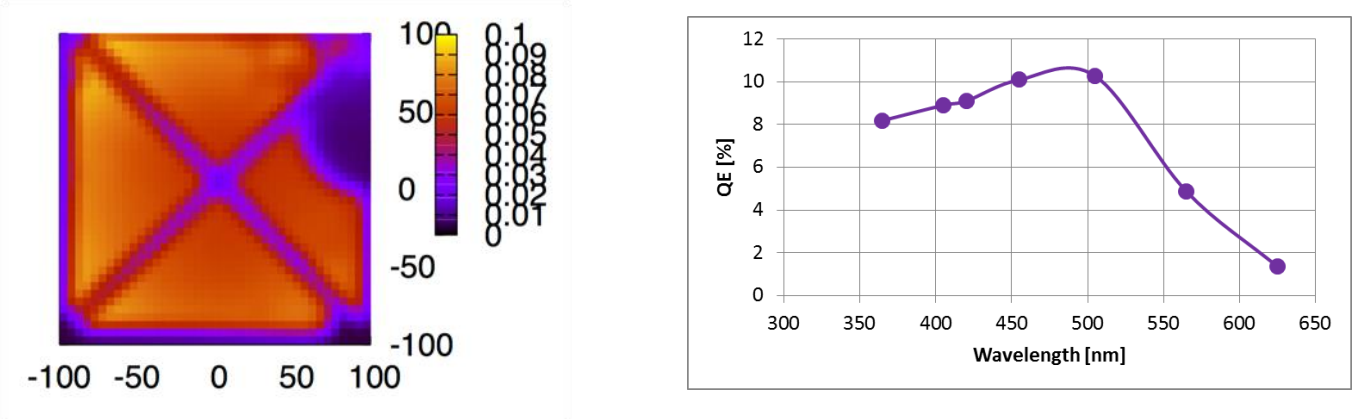


**Figure 6** - **Left**: A photocathode Quantum Efficiency map is shown measured at 365 nm. QE is about 10% at maximum. **Right**: The QE spectrum is shown for a selected location, as a function of wavelength. It was measured as a sealed tile, immediately after fabrication[C].

### Resistive connection between the photocathode and entry MCP

LAPPD #25 has a resistive connection between the photocathode and the entry MCP. This may be a result of a small indium spill, located in the lower right of the QE image in Figure 6. The consequence of the connection is that a bias voltage applied between the entry MCP and the photocathode will drive both a photocurrent and a resistive current. The total current is shown as a function of voltage in Figure 5 in square symbols. The current is collected from the entry MCP, using the entry MCP as an anode near ground (see Figure 3). The photocathode is negatively biased with respect to the entry MCP, so the photoelectrons will leave the

photocathode and be collected on the entry MCP. The current rises with increasing photocathode voltage, but there is an initial, nonlinear increase at voltages below 10 volts.

The contribution of the resistive current may be extracted by applying a positive photocathode voltage, and comparing to the negative voltage ramp. With positive photocathode voltage, the photoelectrons will stay at the photocathode, and only the resistive current will be observed. This ramp is shown in blue circular points in Figure 5. A linear fit through these points has a slope of 6.02 nA/volt, or 166 Mohms. A much better fit is a second order polynomial, which is also shown. This nonlinearity suggests there is non-ohmic conduction between the photocathode and entry MCP.

The difference in currents between the two ramps is shown in the brown circular points. This is the photocurrent. It quickly rises in the first 3 volts, then changes more slowly at higher voltages. This indicates that the photocurrent is nearly completely collected in the first 3 volts. However, the MCPs respond to both the presence of photoelectrons, and their energy. Higher photocathode voltages for the same photocurrent result in a somewhat higher gain as shown in Figure 9.

The resistive connection between the photocathode and entry MCP can result in small changes in MCP current of 2-3 uA as the two voltages are changed independently. This is because both the photocathode and MCP high voltages are linked somewhat through the resistive bridge.

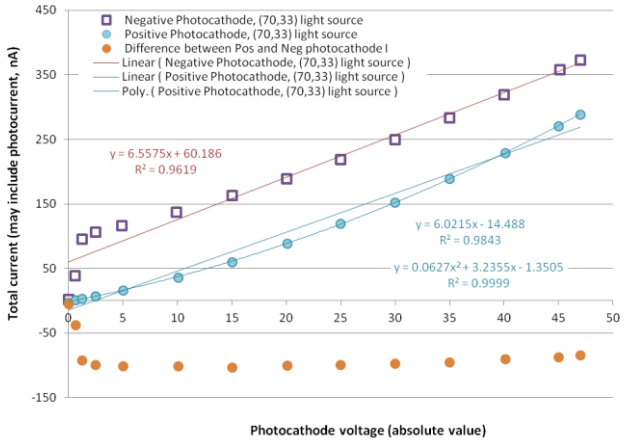


**Figure 7** - The photocathode current is shown vs. the photocathode voltage. A resistive connection of 151 MOhms is present, likely related to a droplet of Indium between the photocathode and top of the entry MCP[D].

### LAPPD Gain vs. MCP voltage

Gain was measured as a function of MCP voltage, using a charge sensitive amplifier and an ADC, and subsequently measured using DRS4 waveform samplers. MCP pulses were produced by directing a 405 nm Edinburgh Instruments 60 pS UV pulsed laser to a selected point on the LAPPD window. The laser was triggered externally at 145 Hz. The trigger pulse was also used to provide a 12 uS window for the ADC, so the pulse height analyzer could detect the LAPPD response from the laser, if there was one, with minimal inclusion of dark pulses. A neutral density filter (NE540B from Thorlabs) was used on the laser to reduce the intensity to the single photon level. The LAPPD responded to 4 out of every 10 laser pulses.

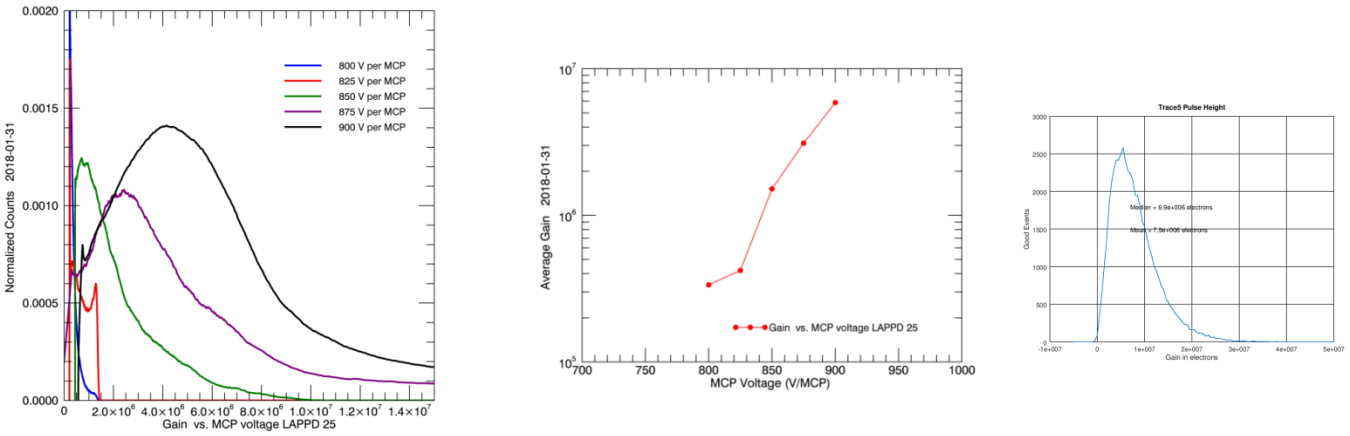


**Figure 8:** Gain is shown vs. MCP voltage, as measured with a charge sensitive amplifier. **Left**: Pulse height distributions for different MCP voltages. **Middle**: Average gain vs. MCP voltage. **Right**: Gain is derived from unamplified charge pulses, as measured with the DRS4 waveform sampler, at MCP voltages 850/950 (entry/exit MCP).

The gain results are shown in Figure 8. Gain is shown vs. MCP voltage, as measured with a charge sensitive amplifier, with gain pulse height distributions for different voltages shown on the left, and average gain vs. MCP voltage in the middle. The gain in the middle panel is the average of the distributions in the left panel. The LAPPD gain for essentially single photoelectrons is as high as 6E6 at 900 volts/MCP. The MCP voltages were the same for both the entry and exit MCPs. The photocathode voltage was 30 volts. The pulse height distributions are peaked.

The right panel of Figure 8 shows the gain derived from unamplified MCP pulses, using PSI DRS4 waveform samplers. In this case, the MCPs voltages were different on the entry and exit MCPs: 850 entry, 950 exit. The photocathode voltage was 50 volts. The gain derived from the DRS4 samples with the 850/950 volt arrangement was 7.9E6.

Gain is shown in Figure 9 as a function of photocathode voltage. There is a tendency for the gain to rise with the increasing energy of the photoelectrons prior to their first strike in the microchannel. This is consistent with the expected increase in the number of secondary electrons from the MgO film as incident electron energy rises (Jokela, 2012).

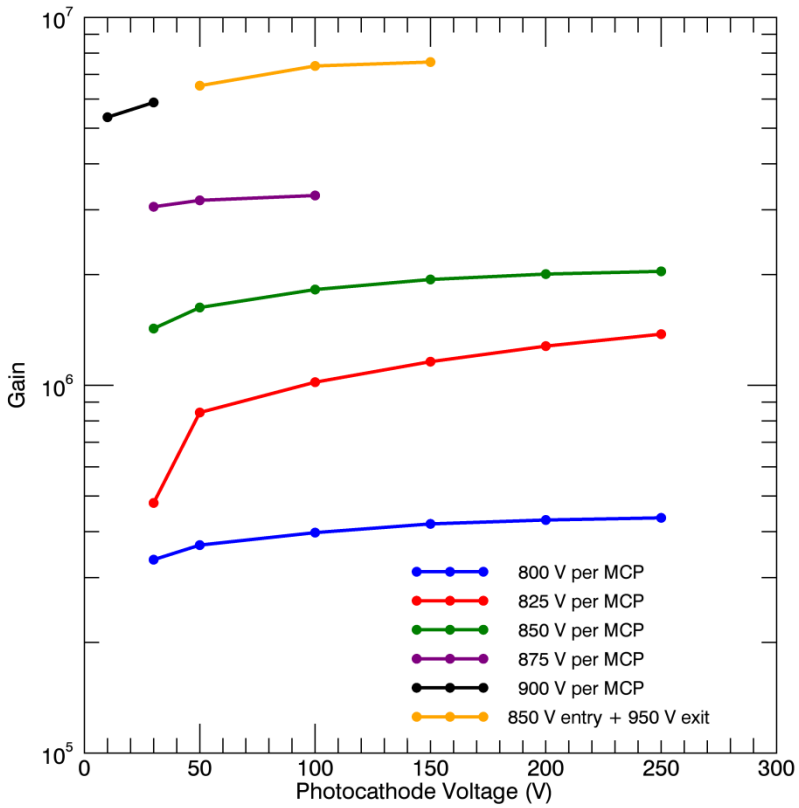


**Figure 9** - Gain is shown as a function of photocathode voltage, at selected MCP voltages.[E]

### LAPPD Gain vs. repetition rate

When a microchannel produces a charge pulse, it needs time to recharge. Otherwise, subsequent pulses will be smaller than the first. The microchannel plates are suitable for high rate conditions because the channels are nearly independent of each other, and unless the same one is struck twice, they will have time to recover.

The reduction of gain as a function of rate was tested by applying the 405 nm laser to a spot on the LAPPD window, of about 1 mm in diameter. The repetition rate was changed, and the corresponding gain was measured. Figure 10 shows the result, in which the gain declines by a factor of approximately two as the rate is increased from 145 Hz/mm^2 to 14,580 Hz/mm^2. Both LAPPD 22 and 25 results are shown in Figure 10 . They have MCPs with relatively low resistance, about 3-14 Mohms, so the MCPs can recharge as effectively as possible. These measurements for LAPPD 25 were made at an MCP voltage of 875 V/MCP, and a photocathode voltage of 50 volts.

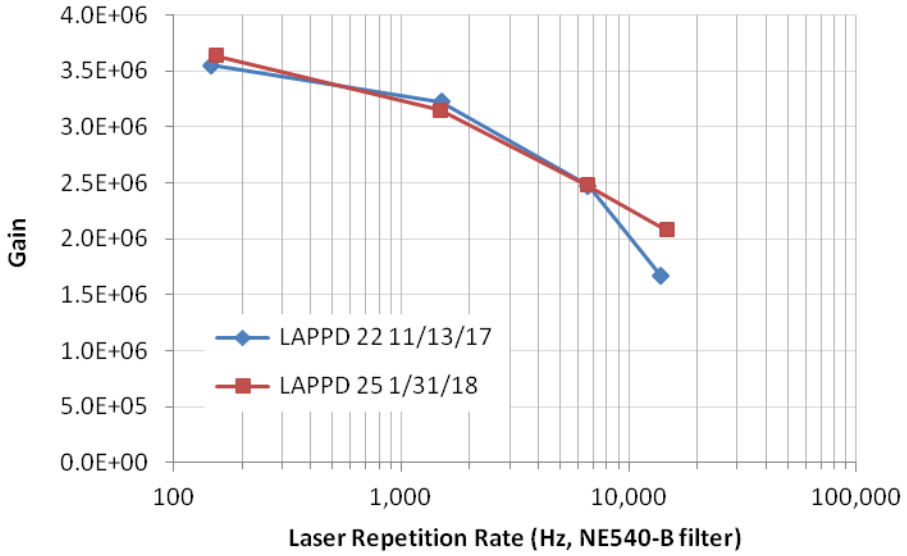


**Figure 10** – LAPPD gain is shown vs. laser repetition rate for single photoelectrons[F].

### LAPPD Dark rates vs. MCP and photocathode voltage

Dark rates are shown in Figure 11 as a function of MCP voltage and photocathode voltage. The higher photocathode voltages tend to increase the gain, but they also increase the dark rates. These rates were acquired from a single strip.

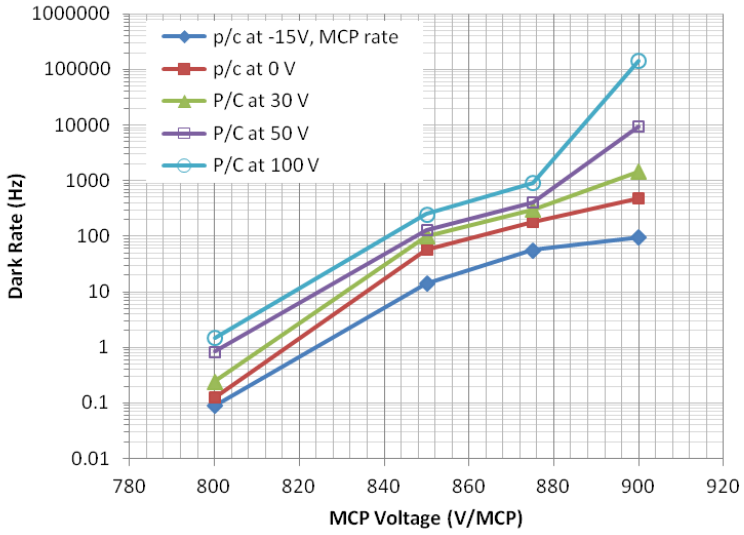


**Figure 11** - Dark rates are shown as a function of MCP voltage, and of photocathode voltage[G].

### Charge Deposition position within the LAPPD

The MCP charge deposition position may be measured with the LAPPD stripline anode in two ways. Along a strip, the position of the charge pulse may be inferred by measuring the relative time of arrival of pulses at

each end of the strip, as the charge deposited by the MCP makes its way to ground at both ends. The time needed for a pulse to travel the entire strip is combined with the difference in arrival time at both ends, and cable offsets are subtracted to calculate the position of charge deposition. This process is shown schematically in Figure 12, right.

A scan of the 405 nm laser along a strip was observed using a pair of DRS4 waveform samplers, and the variation in relative timing therefore measured.

The results of the position scan are shown on the left side of Figure 12. Discontinuities are present at each end, where the laser was near the border of the LAPPD, and on each side of the center, where the laser hit the X-spacer. When the laser light is completely obscured, the observed position is the average of dark pulses, which tends to be near the center.

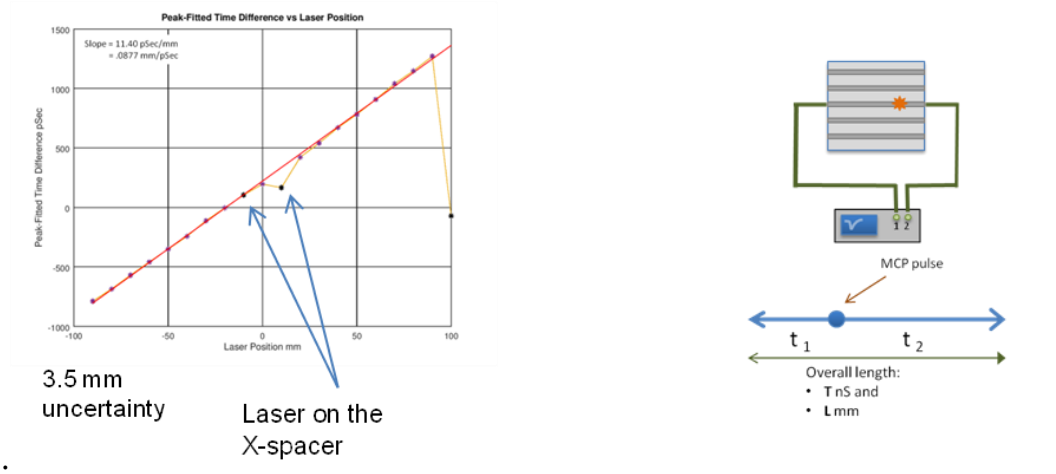


**Figure 12** – Left: Position is inferred from average pulse arrival times at each end of a strip, and plotted against the known laser position. There is a 3.5 mm uncertainty in position. Right: pulses are observed at the left and right ends of a strip. Their relative arrival time leads to position of the charge deposition along the strip.

Position may be measured across strips as well. In this case, the centroid of three adjacent strip signals may be calculated, resulting in the position to a better resolution than the strip pitch itself.

**Timing and position resolution from a scan along a strip using single photoelectrons**

Table 1 shows the test conditions utilized for **Timing and position** characterization of LAPPD #25. Table 2 summarizes the results from scans along and across a strip.

**Table 1** - test conditions utilized for Timing and position characterization of LAPPD #25

| | |
|---|---|
| Photocathode Voltage | -2200 V |
| Entry face of Entry MCP Voltage | -2100 V |
| Exit face of Entry MCP Voltage | -1250 V |
| Entry face of Exit MCP Voltage | -1050 V |
| Exit face of Exit MCP Voltage | -200 V |
| Anode voltage | GND |

**Table 2 – Single Photoelectron LAPPD #25 Performance Summary**

| | |
|---|---|
| Cross-strip Spatial Resolution (across anode strips) | 1.6 mm RMS |
| Along-strip Spatial Resolution (along anode strips) | 2.9 mm RMS |
| Along-strip Time Difference (end-to-end time difference) Resolution | 33.4 psec RMS |
| Along-strip Time Difference (end-to-end time difference) Accuracy | [-2.4 +1.9] mm |
| Efficiency of 10mV threshold | 95% |
| Photon Incident Time Resolution (** UPPER BOUND **) | <200 psec RMS |
| Median Pulse Height (Each end, central strip) | 39 mV |
| Median Pulse Charge (Each end, central strip) | 1.11 pC = 6.9 x 10^6 electrons |
| Baseline Noise Level | 1.3mV RMS |
| Entry MCP Resistance | 14.7 M? |
| Exit MCP Resistance | 10.7 M? |

Using a remotely controlled motor stage, the 405 nm laser was stepped axially at 19 positions along Strip #13 at 1cm separations, followed by a cross-strip stepped scan at 21 positions crossing Strips #12, #13, and #14 at 1mm separations. Each dataset was recorded in binary format using the DRSOsc application as documented in the DRS4 Evaluation Board Operator's Manual.

**Separation of Baseline Null events from Single PE events, and data reduction/compression methods**

Measurement of pulse height distributions and the analysis of spatial resolution along the strip direction required a distinction between electronic noise and MCP pulses. The standard deviation of the waveforms was used to discriminate between the two. The pulses display a marked inflection point on their std-sorted distribution, as illustrated Figure 13 (left). For the cross-strip resolution analysis, where the signal was shared between strips, this method was combined with a simple threshold at >20mV on at least one pulse, on at least one strip, with similar results, Figure 13(right). The latter method was used for the cross-strip resolution results.

The first step in data processing was to correct for a data acquisition artifact from the DRS4 evaluation boards, where random samples gave zero values ("drop-outs"). Values for these samples were interpolated from their neighbors when this occurred. This was followed by a baseline subtraction derived from the average of all samples in all Null events, ignoring observed small pulse-to-pulse baseline variations at the ~1mV level. Pulse magnitude and time values were then derived separately and independently for each pulse on each waveform. The resulting compressed OCTAVE/MATLAB data structures were saved in a separate file for each laser position.

Several "methods" were implemented to define pulse magnitudes and times that were generated in parallel for each pulse on each waveform channel. Parallel analyses were performed using each of these methods/algorithms, generally giving very similar results while providing consistency checks. For the pulse amplitude determination, the following algorithms were executed for each pulse on each waveform:

1. "Magnitude" = the largest amplitude observed for any sample in the waveform;
2. "PeakFit Amplitude" – from Gaussian fit to 5 samples centered on the maximum sample; and "Pico-coulombs" from the pulse integral across a range of bins containing the pulse.

The timing algorithms explored included:

1. "Maximum" - the sample number of the maximal bin;
2. "PeakFit Time" – the time in picoseconds resulting from the above Gaussian fit, and
3. "LeadingEdge" - finding the time in picoseconds where each waveform resampled into virtual 20pSec bins using cubic spline interpolation reached 50% of its maximum on its leading edge.

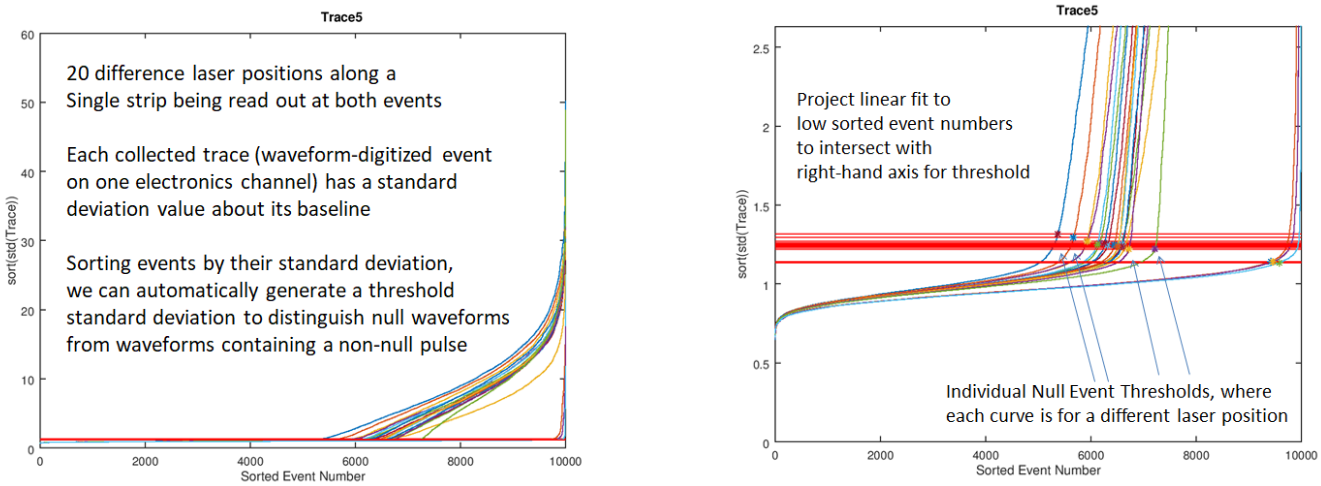


Figure 13 - The methods for distinguishing pulses from background are described

### Along-strip Resolution Analysis and Results

The time-difference distributions for the central strip contained some background contamination from a few events that contained pulses not associated with the laser firing (dark pulses) on the strip being examined or its neighbors. These events appeared as long tails in the timing distribution, which were separated from the strongly peaked time-difference distribution associated with events using an automated thresholding algorithm similar to that used to identify null events. The resulting restricted distribution of pulse time differences for each of the timing algorithms was then separately fitted to a Gaussian for each set of non-null events at each laser position, with the fitted peak value taken as the Time Difference value for that laser position point, and the fitted width taken as the Axial Temporal resolution for that laser position.

A simple, unweighted linear fit of the inferred positions vs. the known laser positions is shown in Figure 14. Two laser positions were excluded from the fit because those positions corresponded to points directly above the X-spacers, where photoelectrons cannot reach the MCPs. The time difference resolution was nearly independent of laser position along the strip, as shown at center below, and had a median value of 37.5 picoseconds = 3.3mm, each RMS, quoted as the device Along-strip Temporal and Spatial Resolution. Residuals from the linear fit, reproduced at lower right, give the accuracy of the Axial Position by simple linear interpolation, based upon pulse time differences. As stated earlier, these results were insensitive to timing method used.

The laser provided a fast pulse indicating when it fired. This pulse could be used as a reference for the arrival of the strip pulses at each end. However, the laser trigger output appears to have insufficient stability for this purpose, giving ~200pSec RMS width average pulse distributions for what was specified as a 60 picosecond width laser pulse on the first (upstream) of the two chained DRS4 evaluation boards. The distribution of the

average pulse times observed on the downstream board was even worse, approaching ~2ns FWHM. This will be addressed in future studies by generating a fast photodiode signal, using split un-attenuated laser light and reading this time reference photodiode signal out through one channel on each of the two chained DRS4 evaluation boards.

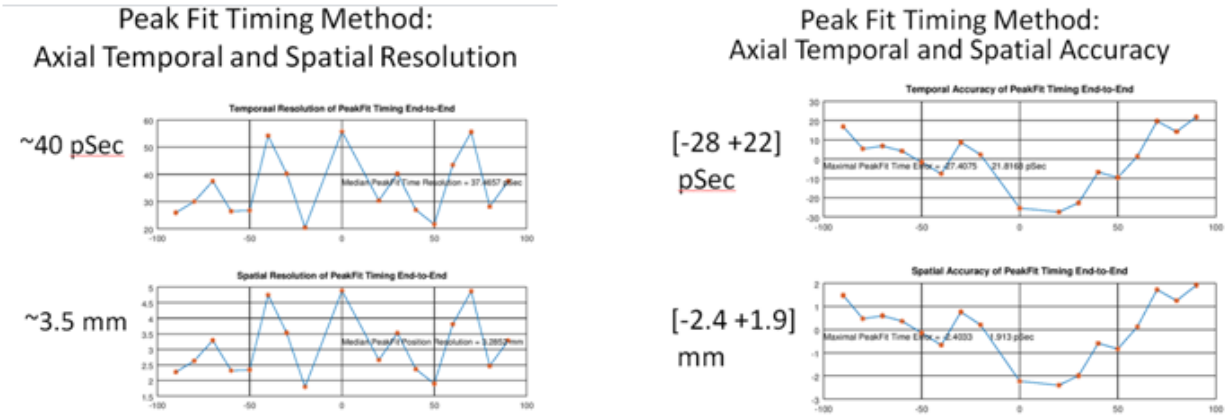


**Figure 14** - Left: Temporal and spatial resolution derived from a scan along a strip is shown. Right: Temporal and spatial uncertainty is shown.

### Cross-strip scan results

Results for the single-photoelectron cross-strip coordinate resolution are shown in Figure 15.

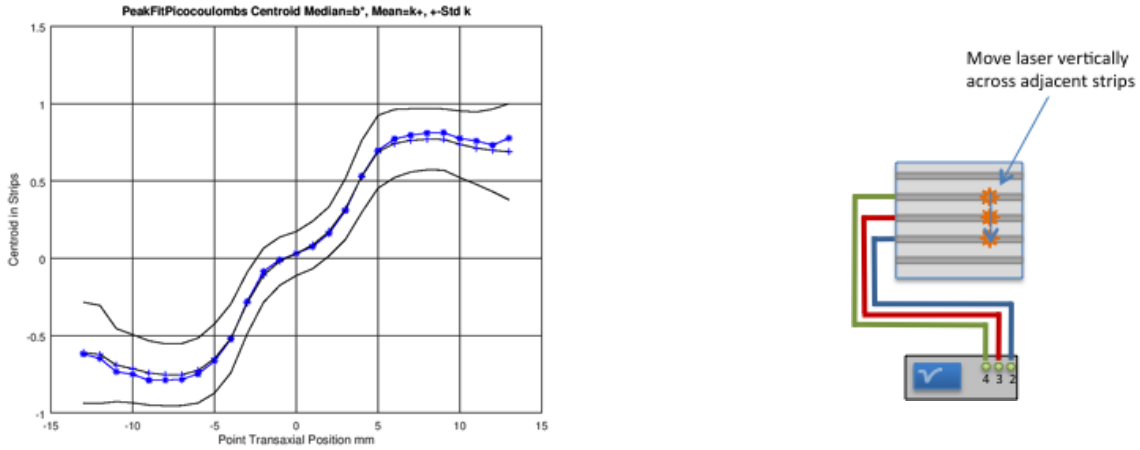


Figure 15 . Left: the position calculated from a cross-strip scan is shown, together with a one-standard deviation uncertainty boundary. Right: Cross-strip measurement direction is shown.

The scan direction is shown in Figure 15 (right). This technique derives position from a centroid calculation that uses three adjacent strips. The centroids were derived using the sum of the waveforms within a restricted range about the pulse peak time ("PeakFitPicocoulombs Centroid") as a function of incident laser cross-strip position. The center of the central strip was taken as zero. Note that since the pitch between strips is ~7mm, only the positions in the range [-3.5:3.5] are strictly valid. On a fully instrumented LAPPD, the peak amplitude for pulses outside this laser cross-strip position range would have occurred on a different strip than on the central strip in the triplet of strips we have used. Extending beyond this valid range yields the "centroid

saturation" observed where the largest pulse was on one of the adjacent strips rather than the central strip. Figure 15 left gives the centroid median (in blue, '*') and mean (in black,'+') which are in good agreement within the valid range of positions. The black curves above and below these show the mean plus standard deviation of the centroid values for events. The pulses used in this analysis had arrival times at the ends of the strips that were consistent with the laser position. This restriction excluded a few background dark noise events. This "cross-strip calibration curve" is expected to be a function of the voltage between the exit MCP and anode, set here to 200V.

---

[A] Onlinemetadata_20180130_Spellman.xlsx, 0V on P/C, 875 V/MCP

[B] Onlinemetadata_20180130_Spellman.xlsx, 0V on P/C, 875 V/MCP

[C] Tile25_QEscan_2018-01-24V0_0.png, in "LAPPD Workshop 1-2018/Photocathode scans" folder

[D] OnlineMetadata_20170810_Spellman with plots.xlsx and OnlineMetadata_20180131_Spellman

[E] OnlineMetadata_20180130_Spellman.xlsx

[F] OnlineMetadata_20180131_Spellman.xlsx, sheet 2; data collected 1/26/18, p.155, Book 3.

[G] See LAPPD 25 data, 1/31/2018